2018-01-01

Characterization Of 3D Printed Polylactic Acid/ Polycaprolactone/titanium Dioxide Composites For Bone Replacement And Grafting

Sandra Elena Najera Beltran
University of Texas at El Paso, snajerab@gmail.com

CHARACTERIZATION OF 3D PRINTED POLYLACTIC ACID/ POLYCAPROLACTONE/TITANIUM DIOXIDE COMPOSITES FOR BONE REPLACEMENT AND GRAFTING

SANDRA ELENA NÁJERA BELTRÁN

Master's Program in Metallurgical and Materials Engineering

APPROVED:

Nam-Soo Kim, Ph.D., Chair

Guikuan Yue, Ph.D.

Jong-Wha Chang, Ph.D.

Charles Ambler, Ph.D.
Dean of the Graduate School

Dedication

It is with my deepest gratitude and affection that I dedicate this thesis to my mother who has always been a source of knowledge and inspiration, and whose encouragement made it possible for me to complete this work.

CHARACTERIZATION OF 3D PRINTED POLYLACTIC ACID/ POLYCAPROLACTONE/TITANIUM DIOXIDE COMPOSITES FOR BONE REPLACEMENT AND GRAFTING

by

SANDRA ELENA NÁJERA BELTRÁN, BS in MME

THESIS

Presented to the Faculty of the Graduate School of

The University of Texas at El Paso

in Partial Fulfillment

of the Requirements

for the Degree of

MASTER OF SCIENCE

Department of Metallurgical, Materials and Biomedical Engineering

THE UNIVERSITY OF TEXAS AT EL PASO

May 2018

Acknowledgements

I would like to thank my advisor and professor Dr. Nam-Soo Kim for letting me be part of his team in the PNE laboratory, and my committee members, Dr. Guikuan Yue and Dr. Jong-Wha Chang. I would like to show gratitude to my colleagues in the Printing Nano Engineering Lab: Dr. Monica Michel, Mr. Eduardo De Ávila, Ms. Diana Cho and all the other members of the team for their support.

This work was supported by the National Research Council of Science & Technology (NST) grant by the Korea government (MSIP) (No. CRC-15-03-KIMM), and by NSF through "NUE: Printing Innovative Nano Technology Research and Elite Education (PINE TREE) Program".

Abstract

A material that mimics the properties of bones was developed by optimizing the ratio of polymer composites of polylactic acid (PLA) and poly-ε-caprolactone (PCL), containing small amounts of titanium oxide (TiO2). Although titanium-based alloys have commonly been used for bone replacement procedures due to their biocompatibility with the human body and their mechanical properties, stress shielding continues to be a problem. The structure of a bone has a porosity which permits the flow of nutrients, blood, oxygen and minerals, and is an issue at the time of creating bone replacements using conventional methods. PLA and PCL have been used in biomedical applications due to their biocompatibility with the human body and their mechanical properties in vivo. PLA and PCL provide strength to the artificial cancellous bone supplying the initial support, and allowing the gradual degradation desired in the human body. In this work the polymer composite materials were prepared, then filaments were used to print the 3D structures using Fused Deposition Modeling (FDM), after which their physical, chemical, mechanical and biological properties were tested. Different characterization methods were used, such as differential scanning calorimetry (DSC), tensile testing, and scanning electron microscopy to evaluate the effect of the fillers. The printed composites show excellent in vitro biocompatibility including cell proliferation, adhesion and osteoblast differentiation and are therefore promising candidates to be used in the field of bio-medical applications. Furthermore, PLA/PCL composites infused with TiO2 seem to be a good option specifically for bone replacement procedures, since the mechanical properties of PLA/PCL/TiO2 composites are similar to the cancellous bones making them a viable option for bone replacement and grafting procedures.

Table of Contents

List of Figures

Chapter 1: Background

1.1 3D printing

Additive layer manufacturing (ALM) is a technology that has been growing rapidly as it has many advantages over conventional manufacturing methods. ALM involves the computer-generated model or computer aided design (CAD) of the desired object and then, the rapid prototyping that includes the solid freeform fabrication (SFF) of such design through one of the different ALM techniques. Stereolithography (SL), digital light processing (DLP), selective laser sintering (SLS), fused deposition modeling (FDM), and multi jet modeling (MJM) are some of the methods used.

Fused deposition modeling is one technology available in the industry, in schools for educational purposes and it is used at home settings. This printing process builds structures by extruding a semiliquid thermoplastic filament layer by layer. This method has various advantages such as the equipment and maintenance costs being low since the structures and devices of the program are simple compared to other printing techniques. For example, with the help of RepRap (Replicating Rapid-prototyper), which is an open source rapid prototyping system, the replication of printer parts can be made and thus the technique applied to a variety of materials. Furthermore, when the precision of the controlling device is augmented, it can be applied to a wider range of industries to strengthen the surface roughness of the models.

3D printing has had an impact in the biomedical field since it provides benefits such as customization of products, cost-effectiveness, and most importantly because it is possible to create complex structures, making it ideal for patient-specific devices. Because of this possibility of creating complex structures, FDM can recreate a structure in which biological components can be incorporated allowing for the regeneration of the bone. The complex nature of the bones with its different porosity areas (cortical and cancellous) can thus be recreated by 3D printing.

1.2 Bone tissue engineering

In the field of tissue engineering, bone grafting has become necessary due to diseases such as arthritis, traumatic injuries, and surgery for bone tumors that are very common, especially in the senior population. Bone grafting is beneficial to repair bones that have been severely damaged or have been lost. Bone replacement may be classified as permanent or temporary depending on the characteristics of its material. A permanent replacement is used when a bone is missing and a temporary implant is used when the implant will be removed after the treatment is successful [1]. The choice of bone graft depends on varying considerations including the intended clinical application, defect size, mechanical properties, availability, required bioactivity (osteoconductive/osteoinductive/osteogenic), handling problem, cost and ethical issues [2].

Once these issues have been considered, the types of grafts can be classified as autograft, allograft and bone graft substitutes, each with its own advantages and disadvantages. Autograft and allograft depend to great extent on the suitability of the donor and constitute essentially the positioning of bones from one place or person, to another. Bone graft substitutes require specific material characteristics and are the subjects of a multitude of studies that focus on engineering substitutes or scaffolds to support bone tissue.

The ultimate tensile strength (UTS) and Young's Modulus of human bones are 60 ~ 120 MPa for compact bones and 7 ~ 25 GPa respectively at different ages [2,3]. The concept of bone tissue engineering includes the design and building of a synthetic frame that will mimic the mechanical properties of the bone. This scaffold should combine mechanical function and tissue generation. Since bones are not homogenous, but formed by bone tissue that varies in composition and porosity, the scaffolds that will support or replace them should be adequately designed [4]. The mechanical properties depend upon the porosity, size and distribution of hydroxyapatite (HA) crystals within collagen fibrils, and the presence and distribution of micro cracks within the bone. The collagen fibril matrix provides both toughness and tensile strength and the crystalline HA structure provides compressive strength and brittleness. Because of this, the optimization of porosity needs to mimic the superficial cortical (high density tissue) and the internal cancellous

(more porous) bones. The mechanical and biological performance of scaffolds depends on the integration of the computational topology design, the solid free form fabrication and the material used to fabricate it [5,6]. To initiate the development of materials for bone grafting, the scaffolds should be fabricated, then tested for their mechanical characteristics and, beyond that fabricated scaffolds needed to be validated as appropriate candidates to be used in animals as well as in the human body.

The process of grafting is expensive because it usually includes metal substitutes such as stainless steel, magnesium, titanium or cobalt alloys, and this method of using metal has had some problems due to factors such as the metal's higher strength and toxicity. Some kinds of metal ions (titanium, aluminum, vanadium, nickel, cobalt, chromium) released over a period of time are toxic in the human body, and even if some of them are normal components of the body, they can become toxic at high dosage [7]. When the strength of the bone is less than the transplanted support, the bone will most likely break instead of the implant, since the implant carries most of the load resulting in a weakening of bone (stress shielding). For these reasons, temporary grafting is preferred, eliminating or replacing it as needed.

Biodegradable materials have emerged to solve these problems [8]. Taking advantage of the regenerative character of bones, implants or grafts no longer need to be removed thus minimizing trauma and risks of infection from secondary surgeries. The biodegradable scaffold can degenerate and eventually disappear as new tissue is growing and regenerating. Biodegradable magnesium alloys, ceramics and polymers make suitable scaffold building materials.

1.3 Biomaterials

Polymer materials can be natural such as collagen and chitosan, or synthetic, i.e. polylactic acid (PLA), polyglycolic acid (PGA), poly-ε-caprolactone (PCL) and poly-β-hydroxybutayrate (PHB) as well as polylactic acid-c—glycolic acid (PLGA) [9]. Polymers in both categories have been used for medical applications [10–12]. PLA and PCL, the polymers used in this study, are synthetic biodegradable thermoplastic polymers these two polymers have been used in the field of

biomedical applications due to their biocompatibility with the human body, and their mechanical properties in vivo [13,14]. Specific properties can be obtained when different polymers are mixed and can be tailored depending on the application in which they will be used.

PLA can be blended with other flexible polymers that will act as plasticizers to improve its toughness and reduce its brittleness [15]. PCL is a biocompatible and biodegradable aliphatic polyester like PLA. It has good toughness, displays rubbery properties and has low glass transition and melting temperatures. It is also more thermally stable than PLA, which opens the possibility that the presence of PCL in PLA will not only improve its toughness, but also its thermal stability. When it is blended with PCL, the brittleness of PLA is improved [16]. The possibility of the application of these two polymers as bone graft scaffolds and biomaterials is growing since they complement each other in their physical properties and biodegradability.

Titanium dioxide (TiO_2) particles can be added into the composite to obtain even more favorable material properties such as toughness, flexibility and thermal stability [17]. Although TiO_2 is an inorganic particle, it exhibits suitable biocompatibility and is well known to be non-toxic depending on crystalline phase, the size of the particles and condition of aggregation [18,19]. Anatase and rutile are two phases of TiO_2 particles with different properties. Several studies have reported that anatase particles show lower toxicity than rutile particles [20]. It has also been discovered that particles smaller than 20 nm show higher toxicity than larger particles [21]. Another factor that has to be considered is the aggregation of the particles; aggregates ~600 nm show higher effect on cell viability than smaller aggregates of ~160 nm. Titania, with its antibacterial characteristics [22], helps reduce the risk of infections from implants in the body. The TiO_2 can serve as filler for additional reinforcement and to increase the polymer's mechanical properties. The addition of TiO_2 into the materials requires the particles to be scattered uniformly into the blend to prevent bulging of the material [23].

Chapter 2: Materials and structures

2.1 Materials

The polylactic acid in pellet form used in the study was a commercial grade (PLA 4043D), with a density of 1.24 g/cc, glass transition temperature of ~53°C and a melting temperature of ~153°C. The polycaprolactone also in pellet form (Sigma-Aldrich, St. Louis, MO) has a density of 1.15 g/cc at 25°C, a glass transition temperature of ~60°C and a melting temperature ~65°C. The titanium dioxide (Sigma-Aldrich, St. Louis, MO) of three different sizes (50 nm, 150 nm and 300nm as seen in figure 2.1), were received as anatase with melting point of ~1800°C, and a density of 4.26 g/cc at 25°C. All materials were used as received.

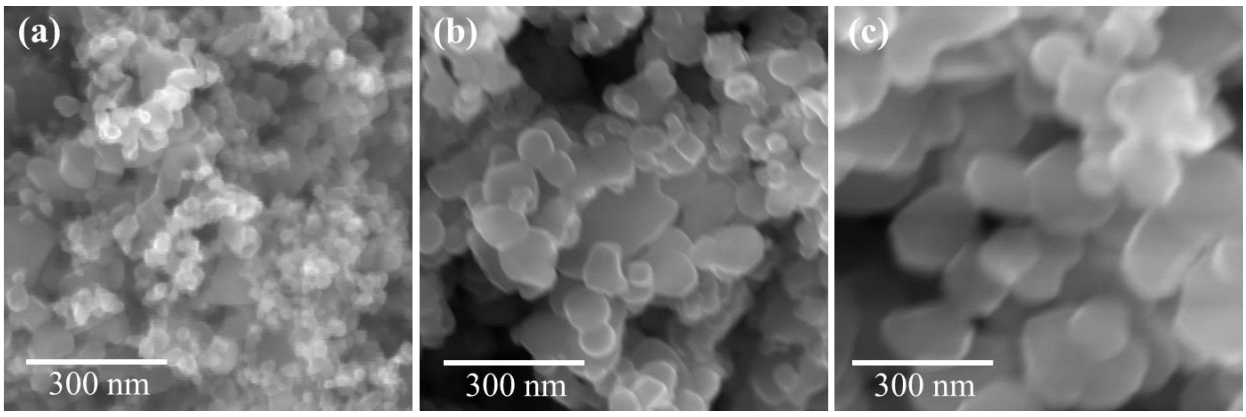

Figure 2.1: SEM images of titanium dioxide particles for this study. (a) Small (50 nm), (b) medium (150 nm), large (300 nm).

2.2 Filament preparation

To make the filament, a blend was prepared to make pellets with the desired composition. The first blends made were a mixture of PLA/PCL with different compositions (75/25 wt. %, 50/50 wt. % and 25/75 wt. % PCL). After testing their mechanical properties, the blend composed of 75 wt. % PLA and 25 wt. % PCL showed the best characteristics. This composition was the one selected to study the effect of the addition of titanium dioxide. The mixing process starts by first melting the corresponding amount of PLA due to its higher melting point. PCL is then added, and when the blend is uniformly mixed, the filler is added and stirred until a homogeneous mixture is

achieved. The solid mixture is then cut into pieces small enough to be fed into the filament extruder (figure 2.2). The extruder consists of a motor, a pellet feeder, a heated barrel, a screw and a die. The motor rotates the screw inside the barrel and directs the pellets to the end of the barrel. With the help of a heating band, the material melts and is extruded through the die or nozzle into a filament. The barrel has a length of 15 cm and an outer diameter of 2.5 cm. The screw has the same length with a diameter of 2 cm, while the nozzle of the extruder has a diameter of 2 mm. The filament, after being extruded, has a diameter smaller than 2 mm allowing it to fit into the print head of the 3D printer. The filament extruder and the printer used were developed by members of the PNE laboratory (figure 2.3), who have been developing and improving printing methods with different materials [24–30].

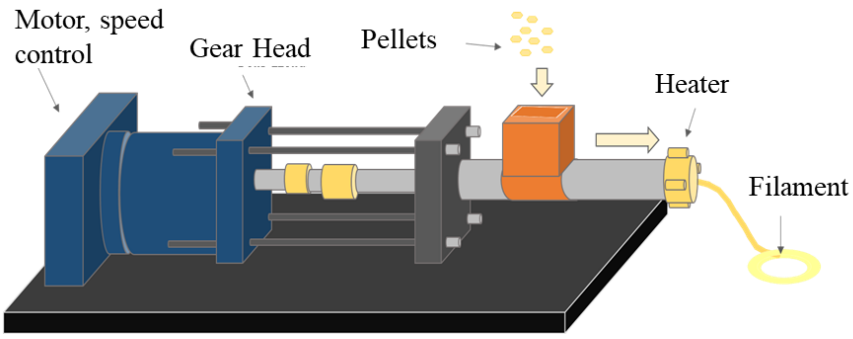

Figure 2.2: Extruder used to make filaments developed in the PNE laboratory.

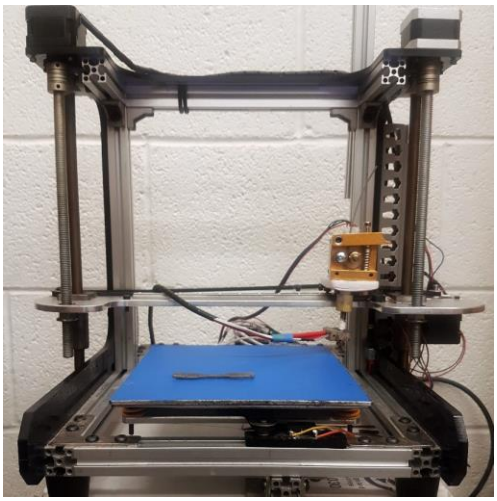

Figure 2.3: 3D printer used to fabricate testing samples developed in the PNE Laboratory.

2.3 Structure fabrication

The filaments made of various compositions of PLA, PCL and TiO_2 were used to print specimens for tensile testing. Specifications for sample preparation followed the standards of the American Society for Testing and Materials (ASTM) D638 type IV (figure 2.4), and the outer structure of the artificial bone was also printed (figure 2.5). Fused Deposition Modeling (FDM) consists of continuous addition of thin layers of material, in which the filament is placed into the heated extruder and according to the 3D data the material is extruded through a nozzle to 3D print the cross section of the desired object into a heated platform. The melted filament layers will then bond to the previous layers as they solidify. The printing process for all different filaments was maintained constant with the same printing parameters. Tensile samples used to test the polymer-polymer interface were made using a similar printer but with two nozzle heads instead of one. The process is the same, only the code is modified so that the printer alternates between two different nozzles, each with its own filament, using only one extruder at a time, controlling different temperatures and printing speeds. The quality of the final print is dependent on the temperature, speed and the layer thickness.

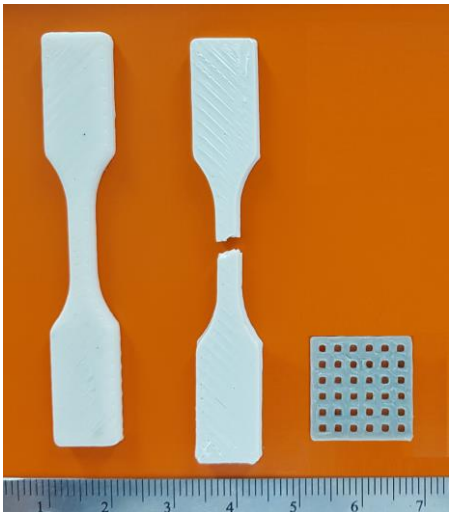

Figure 2.4: Structures printed for tensile and biological tests.

Figure 2.5: 3D printed model of cancellous bone with PLA/PCL/TiO_2 74.25/24.75/1 wt.% composite.

2.4 Material interface analysis

A polymer blend interface is when a polymer is in contact with another polymer and a polymer composite interface is when it is in contact with filler or other non-polymer materials. The blends of PLA and PCL are immiscible because of the resulting low entropy and the heat of mixing which is frequently positive [31]. According to Helfand and Tagami, an interface is when the molecular species occupy a space of a very small length, and the composition in these phases varies [32]. The interface area of two polymers increases when they are mixed in powder state. Since in this work PLA and PCL were melt mixed, they have a low interface, but much higher than the samples made using a dual nozzle head. The mechanical behavior between different interfaces can be described in terms of thermodynamics.

Tensile strength samples were designed to get the same 50:50 ratio with different number of interfaces. This ratio was chosen because at this point the samples would have the maximum value of ΔS. To study the effects of interface areas, the overlapping gauge was changed as illustrated in figure 2.6. When the number of interfaces is higher (sample C), the interface area increases dramatically. In this study, the change in tensile strength was studied according to the change (increase) in the interface area.

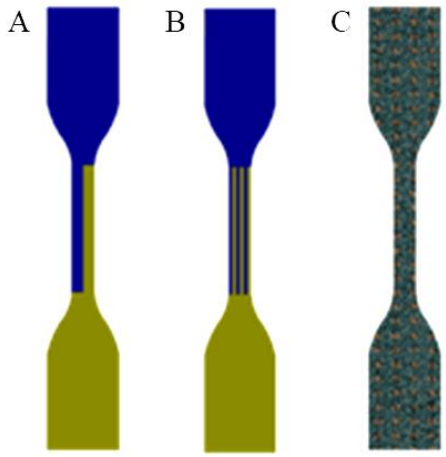

Figure 2.6: Interface areas of printed samples 1:1 PLA/PCL. Interface images A and B printed using dual nozzle printer and image C printed with melt mixed material.

Chapter 3: In vitro analysis

3.1 Cell culture

Mouse calvarial isolated preosteoblast cell line, MC3T3-E1 subclone 4, were grown in alpha-MEM (Gibco, Gran Island, NY) supplemented with 10% fetal bovine serum 100 U/ml penicillin and 100 μg/ml streptomycin (Gibco, Gran Island, NY) under a humidified atmosphere of 95% air / 5% CO_2 at 37°C. Cells were subcultured 2-3 times per week, and the medium was changed every other day. To obtain osteoblast, cells were cultured in α-MEM containing 50 mg/L of ascorbic acid, 10 mM β- glycerphosphate, and 50 ng/ml of BMP2 (Sigma-Aldrich, Sr. Louis, MO). All the PLA/PCL/TiO_2 composites were sterilized with 2X antibiotics solution (2% penicillin and streptomycin) for 1 hour at room-temperature and pre-incubated in growth medium for 3 additional hours at 37°C.

3.2 Cell proliferation assay

Cell proliferation assay was performed using Celltiter 96® aqueous one solution cell proliferation assay (Promega, Madison, WI) according to the manufacturer's instructions. Cells were seeded in the 96-well culture plate at 1 x 103 cells/well with PLA/PCL/TiO_2 composites. At days 1, 2, 5, 7 and 14 a 10 μl/well of MTS reagent was added for 2 hours at 37 °C to allow the formation of a soluble violet formazan product by viable cells. MTS-1 reagent is a stable tetrazolium salt. When it is cleaved into soluble formazan by a dehydrogenase such as succinate-tetrazolium reductase, it detects only viable cells. Therefore, the optical density of violet formazan dye is correlated directly to the number of cells. The absorbance was determined to be 490 nm using a microplate spectrophotometer (BioTek, Winooski, VT).

3.3 Immunofluorescence

Cells were cultured onto a 12-well culture plate at a density of 1 x 104 cells/well in the PLA/PCL/TiO_2 composites or a poly-D-lysine coated coverslip. For filamentous-actin staining, cells were washed with PBS and fixed with 10% neutral buffered formalin (Sigma-Aldrich, Sr. Louis, MO) for 15 min. Cells were then treated with 0.1 % Triton X-100 for 5 min at room

temperature and reacted with Rhodamine-conjugated phalloidin (Molecular Probe, Eugene, Oregon) for 2 hours at room temperature. To protect the fluorescence signals and make the nuclei visible, cells were mounted with DAPI containing mounting solution (Vector Laboratories, Burlingame, CA). All fluorescence images were captured by a LSM 700 confocal microscope (ZEISS, Jena, Germany).

3.4 Alkaline phosphatase (ALP) and alizarin red S staining

For ALP staining, MC3T3-E1 cells were cultured in 48-well culture plate at a density of 1 x 105 cells/well. After osteoblast differentiation using conditioned medium, alkaline phosphatase staining was performed using Leukocyte alkaline phosphatase kit (Sigma-Aldrich, Sr. Louis, MO) according to the instruction. Cells were immersed in a fixative solution (2.5 ml of citric acid, 6.5 ml of acetone and 0.8ml of 37% formaldehyde) for 1 min, rinsed with distilled water, and incubated with Naphthol-AS-BL alkaline solution mixture at room-temperature for 30 min. Cells were additionally rinsed with distilled water and air dry. For alizarin red S staining, cells were plated in 48-well culture plate at a density of 1 x 105 cells/well. After being fixed in 10% neutral buffered formalin for 15 min at room temperature, cells were rinsed with distilled water and stained with 2% Alizarin Red S solution (Millipore, Billerica, MA) for 30 min, washed again, air dry images were photographed.

3.5 RNA extraction and real-time PCR

Total RNA was extracted using Trizol reagent (Sigma-Aldrich, Sr. Louis, MO) and cDNA was synthesized by M-MLV reverse-transcriptase (Promega, Madison, WI). To quantify the relative mRNA expression of osteogenic markers, the primer for ALP (forward; 5'-CCAACTCTTTTGTGCCAGAGA-3', reverse; 5'-GGCTACATTGGTG TTGAGCTTTT-3'), osteocalcin (forward; 5'-GCAATAAGGTAGTGAACAGACTCC-3', reverse; GTTT GTAGGCGGTCTTCAAGC-3') and GAPDH (forward; 5'- AGGTCGGTGTGAACGGATTTG -3', reverse; 5'- TGTAGACCATGTAG TTGAGGTCA-3') were used. Diluted cDNA by one over two was mixed with 1 X SYBR green master mix (Applied Biosystems, Foster city, CA) and 0.2

μM forward and reverse primers. Quantitative RT-PCR was performed using StepOne real-time PCR (Applied Biosystems, Foster city, CA) and normalized by GAPDH levels.

Chapter 4: Analysis tools

4.1 Differential scanning calorimetry (DSC)

The heat flow of the composites was analyzed using a differential scanning calorimeter as the one in figure 4.3 (DSC 404 F1 Pegasus®, NETZSCH, Germany) to confirm whether PLA and PCL exhibit miscible or immiscible behavior. The scan speed was constant at 5 °C/min by using controlled mixed gases. The setting temperature of the blended PLA/PCL and PLA/PCL/TiO_2 was determined by following the DSC results.

Figure 4.1: Netzsh DSC 404 F1 Pegasus differential scanning calorimeter [33].

4.2 Scanning electron microscopy (SEM)

The fracture surface of the composites was observed using a SEM (Hitachi Tabletop TM-1000, Japan). This microscope (figure 4.2) uses a beam of electrons to generate signals at the surface of solid specimens and it is able to show the texture and the chemical composition of the sample. The samples were cut parallel to the fracture surface having a height of approximately 5 mm. They were mounted on the holder using double-sided conductive carbon tape; no coating was needed to examine the specimens

4.3 Energy dispersive spectroscopy (EDS)

Elemental or chemical analysis was performed using an EDS (figure 4.2) dedicated for Hitachi TM-1000 Tabletop Microscope (SwiftED-TM, Japan) to determine the dispersion and distribution of the filler particles in the composite. Images generated by the backscattered electrons in the SEM reveals the difference in atomic number and are also used for element mapping to detect particular elements and their dispersion and intensity.

Figure 4.2: Hitachi TM-1000 Tabletop scanning electron microscope with EDS [34].

4.4 Tensile test machine

Tensile testing is used to see how samples behave when forces are applied in tension, and to define the material as brittle or ductile. TestResourses 100 Family Universal Test Machine (figure 4.1) was used to perform the test for all samples. A tensile profile is created during the test and the results are graphically shown in a stress-strain curve. All the tests were conducted at room temperature.

Figure 4.3: TestResourses 100 Family Universal Test Machine [35].

4.5 Microplate spectrophotometry

Cell concentration in the composites was studied using a microplate spectrophotometer (BioTek, Winooski, VT). This analytical instrument (figure 4.4) measures the reflection of visible light, UV light or infrared light as a function of its color (wavelength). Since all chemical compounds absorbs or reflects light differently, spectrophotometry can determine the concentration of a known substance by detecting the intensity of the light. This absorption or reflection is determined by capturing and evaluating the color observed with the instrument.

4.6 Confocal microscopy

To study the three-dimensional dynamics in living cells a confocal microscope (ZEISS, Jena, Germany) and immunofluorescence staining were used. This microscope (figure 4.5) creates images by excluding most of the light from the specimen that does not come from the microscope's focal plane and illuminates it by the excitation of fluorophores causing detectable fluorescence. A

confocal microscope differentiates from a conventional microscope since it gives better contrast, more color possibilities, three-dimensional reconstruction of specimen, and improved resolution.

Figure 4.4: Epoch Microplate Spectrophotometer [36].

Figure 4.5: ZEISS LSM 700 confocal microscope [37].

4.7 StepOne real-time PCR

To quantify the relative mRNA expression of osteogenic markers, RT-PCR was performed using StepOne real-time PCR (Applied Biosystems, Foster city, CA). This PCR system (figure 4.6) is used to amplify a small segment of DNA by making a sequence of millions of copies of this segment. This technique is used to reproduce large segments of DNA using few cells instead of instead of making unnecessary use of many cells.

Figure 4.6: StepOne real-time PCR system [38].

Chapter 5: Results and discussion

5.1 Thermal analysis

Differential scanning calorimetry was used to determine critical temperatures of the materials such as melting and crystallization. Results also showed that the two polymers used are immiscible. Figure 5.1 shows melting endotherms of PLA and PCL which appear at 66°C and 183°C, respectively. For the blend with a 3:1 ratio of PLA and PCL, there are two peaks for the melting temperatures which demonstrate these polymers are immiscible. The presence of PCL in the blend does not affect the melting temperature of the PLA. Crystallization exothermic peaks are located at the range of 90°C to 100°C for the 3:1 mixture meaning that PCL increases the crystallinity. This crystallization behavior is common in PLA, and it controls the degradation rate and the mechanical properties [39]. It has been reported that higher amounts of crystallinity in a material improve its mechanical properties [40]. In addition, the increased stability of the polymers by the addition of TiO_2 has been proved in this study. The particles of TiO_2 have improved the stability of PLA without affecting melting temperature through the enhanced interaction between PLA and the particles.

5.2 Elemental analysis

To identify the presence of TiO_2 in polymer matrix, EDS analysis was performed. Elements from our materials generate different energy values. The computer compares these values with standard energy values. Variations in the intensity of the energy values indicate a relative concentration of the selected elements. Two samples were analyzed using this technique to determine TiO_2 dispersion (size and shape of the particle) and distribution (spreading) in the material. The first sample was a small segment of filament composed of PLA/PCL with 1 % TiO_2 medium particles, and the second sample was a small printed cube (5 x 5 x 5 mm).

The cross section of the filament and the top side of the printed sample were analyzed in the SEM and then the EDS spectrum was compared with known standards. Results of the analysis are shown in figure 5.2. The left side of the figure shows SEM image and the corresponding

elemental maps of the cross-section of the filament. These maps show how TiO_2 particles have good dispersion and relatively good distribution. The right side of figure 5.2 groups the elemental maps and SEM image of the printed sample, and they also show good dispersion and better dispersion compared to the filament sample.

From these results, it can be said that the preparation of the blends and the filament extrusion generate a material with homogeneous composition, and that the fabrication of the structures using fused deposition modeling enhances the distribution of the particles in the polymer matrix.

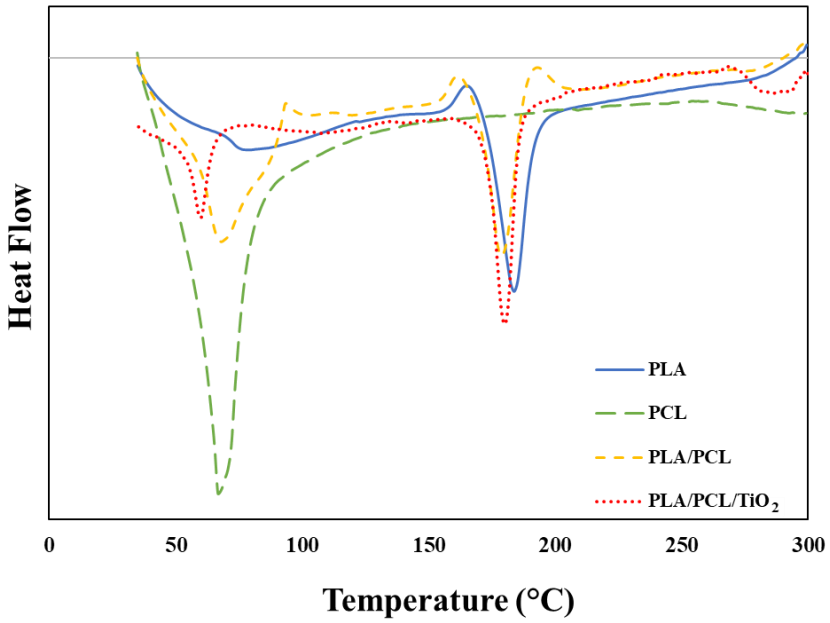

Figure 5.1: Differential scanning calorimetry (DSC) measurements of PLA 100 wt.%, PLA/PCL 75/25 wt.%, PLA/PCL/TiO_2 74.25/24.75/1 wt.% and PCL 100 wt.%.

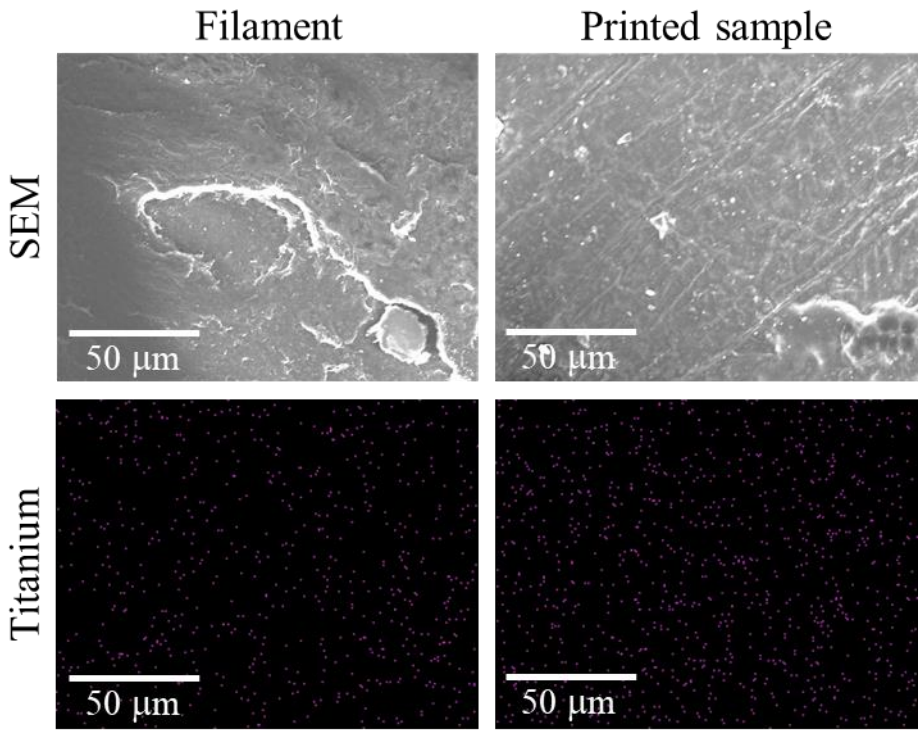

Figure 5.2: EDS mapping of the cross section of a filament, and a printed sample, both composed of PLA/PCL/TiO_2 74.25/24.75/1 wt.%.

5.3 Effect of interface area in PLA/PCL blends

Mechanical behavior of PLA/PCL interface

The effect of the different types of interfaces on the tensile strength is shown in figure 5.3. Samples labeled in the figure are composed of PLA/PCL 50/50 wt. %, but with different type of interface areas. Sample A and B were printed using a dual nozzle head printer and they have different interface patterns; sample A has an interface area of 0.2 mm^2/g, and sample B, 0.7 mm^2/g. A greater interface area is expected when polymers are melt mixed, and this can be observed in sample C with 24.2 mm^2/g, assuming the radius cluster of PLA is 100 µm. Larger interface areas enhances stronger adhesion forces that improve the mechanical properties of the blends giving a better reinforcement to the system [41]. The tensile strain shows that the samples with a larger interface area will elongate more. Sample C exhibits the highest ultimate tensile strength of the three samples, this value (18 MPa) is much lower than the theoretical value for a mixture of PLA

and PCL since they show high immiscibility. The interface between pure PLA and PCL is expected to have the same effects from melt blending technique during the printing process.

Fractography of PLA/PCL interface

The partial rupture of the PLA and PCL for different types of interface can be seen in the SEM images (figure 5.4). Micrographs of samples A and B show how the bonding force between PLA and PCL holds some portions of the material giving smaller elongation, and how the portions of pure PCL have greater elongation. The sample C showed a different type of fracture. It can be seen in the corresponding micrograph that this sample doesn't show different elongations for the two polymers since it was melt mixed.

These results show that in specimens A and B the stronger parts were the interface lines. However, PLA/PCL interface lines are not as strong as the melt mixed material. Therefore, the tensile strength shows to be better with larger interface area because it creates stronger bonding forces.

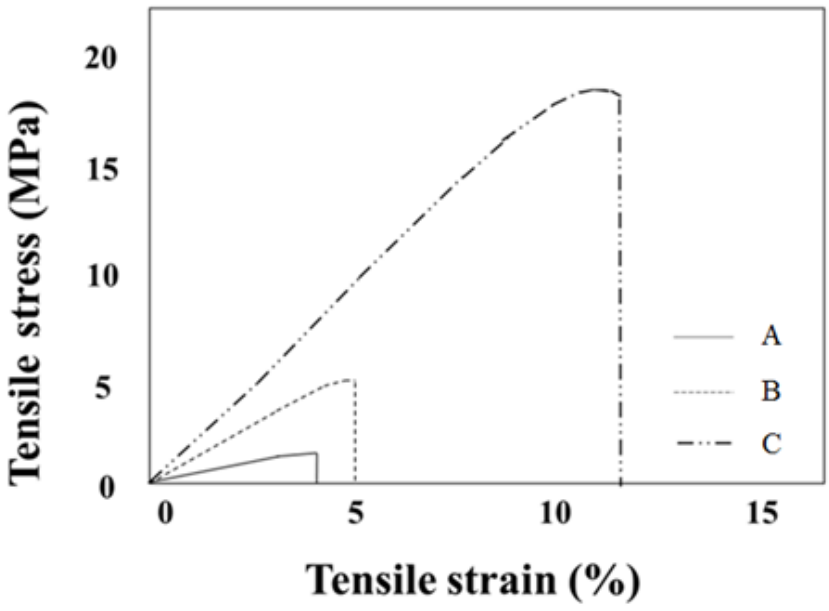

Figure 5.3: Stress-strain curve for 1:1 PLA/PCL with different interface areas (A: 0.2 mm^2/g, B: 0.7 mm^2/g., and C: 24.2 mm^2/g).

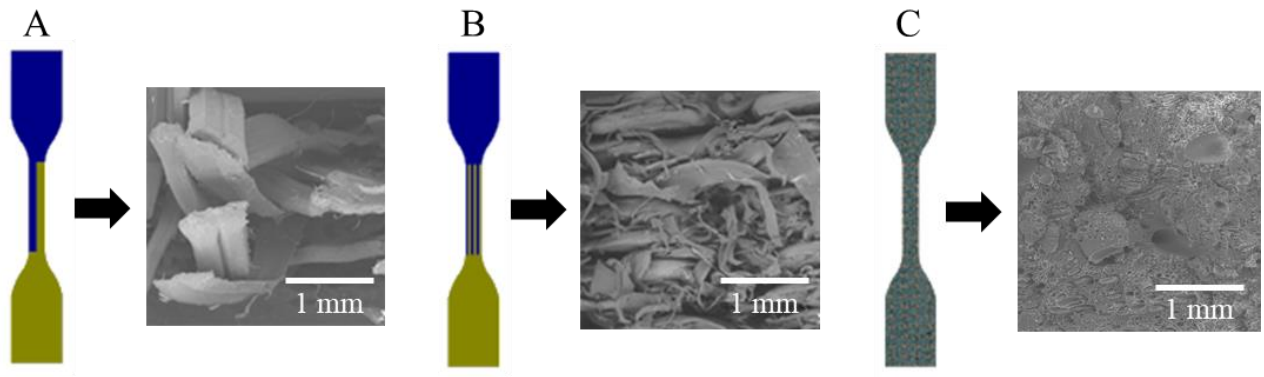

Figure 5.4: SEM images of 1:1 PLA/PCL with different interface areas (A: 0.2 mm^2/g, B: 0.7 mm^2/g., and C: 24.2 mm^2/g).

5.4 Effect of blend composition

Mechanical behavior of PLA/PCL blends

To demonstrate the mechanical properties of PLA/PCL composites, tensile test was performed. Figure 5.5 depicts the stress and strain curves of PLA/PCL filament. The graph shows the strength of the polymers improving with increasing percentage of PLA. The slope of the strain-stress curves indicates Young's modulus which is the degree of deformation and elongation of the samples when subjected to tensile stress. As the content of PCL increased, the Young's modulus and ultimate strength (UTS) decreased whereas tensile strain was increased. In other words, the blends with lower concentration of PCL are more rigid and have smaller deformation. The fracture images in figure 5.6 are consistent with the stress and strain curves which show more ductile behavior when PCL content is higher.

It has been suggested that immiscible blended materials present poor mechanical behaviors; in this work however, the weight ratio of PLA/PCL 75/25 wt. % showed the highest tensile stress compared to the other composites. The mechanical properties can be modified depending on the blending process such as melt blending technique [42]. In the present study, it has been proved that the tensile stress and strain can be controlled by the amount of PCL during the blending process.

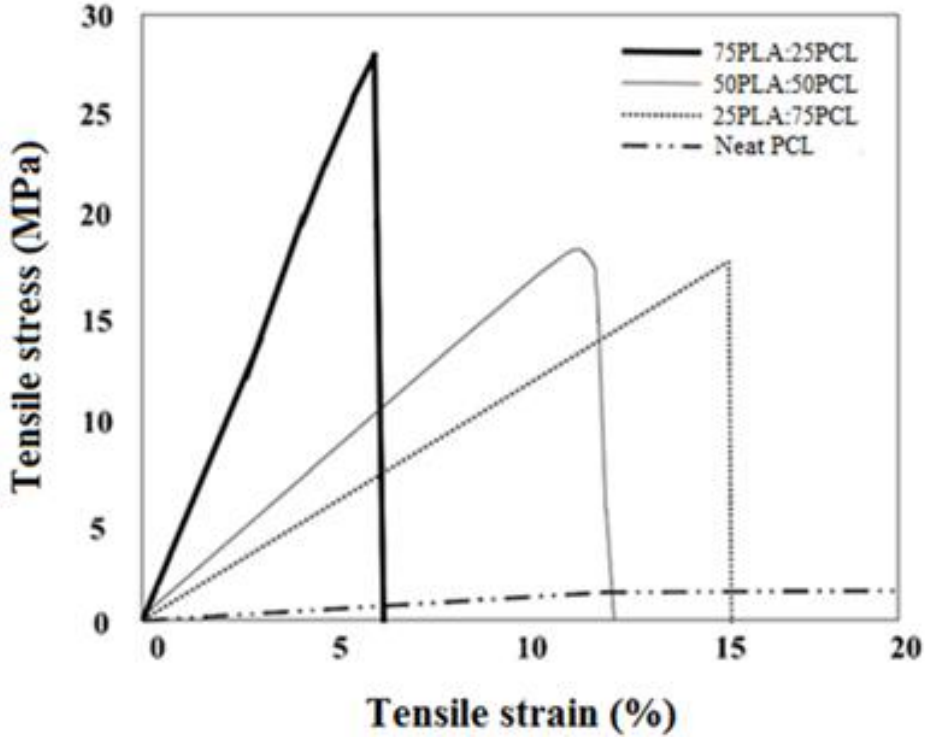

Figure 5.5: Stress-strain curves for different compositions of PLA/PCL (PLA/PCL 75/25 wt.%, PLA/PCL 50/50 wt.%, PLA/PCL 25/75 wt.%, and PLA/PCL 0/100 wt.%).

To explore the mechanical properties of PLA/PCL composites, hardness test was also performed, and results show that the hardness generally decreased when the amount of PCL was increased (data not shown). However, the hardness of PLA/PCL 75/25 wt. % was higher compared to PLA/PCL 50/50 wt. %. The hardness can be affected by the porosity within the structure and this explains why there is fluctuation in the pattern of hardness.

Surface analysis of PLA/PCL blends

Images taken with the SEM show the surface of the specimens from different composition ratios. As shown in figure 5.7, there is very little or no spacing on the surface of PLA/PCL blends at the weight ratio of 100/0, 75/25, 25/75 wt. % which means there is good bonding between the fibers (figure 5.7a-c). The sample composed of PLA/PCL 75/25 wt. % (5.7b) appears to have a rougher surface due to the high mixing energy between these immiscible polymers giving them

higher strength. This is consistent with tensile results in figure 5.5. On the other hand, the surface of PLA/PCL blends with 0/100 wt. % shows some space between fibers and it may occur by the fixed range of 3D printing temperature from 150°C to 200°C and the fact that the materials had been extruded in a liquid state which may cause the structure to shrink as it solidifies (figure 5.7d).

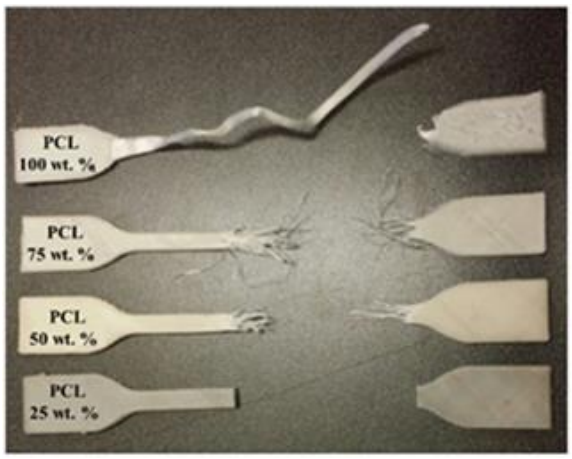

Figure 5.6: Fracture images corresponding to stress-strain curves in figure 5.5.

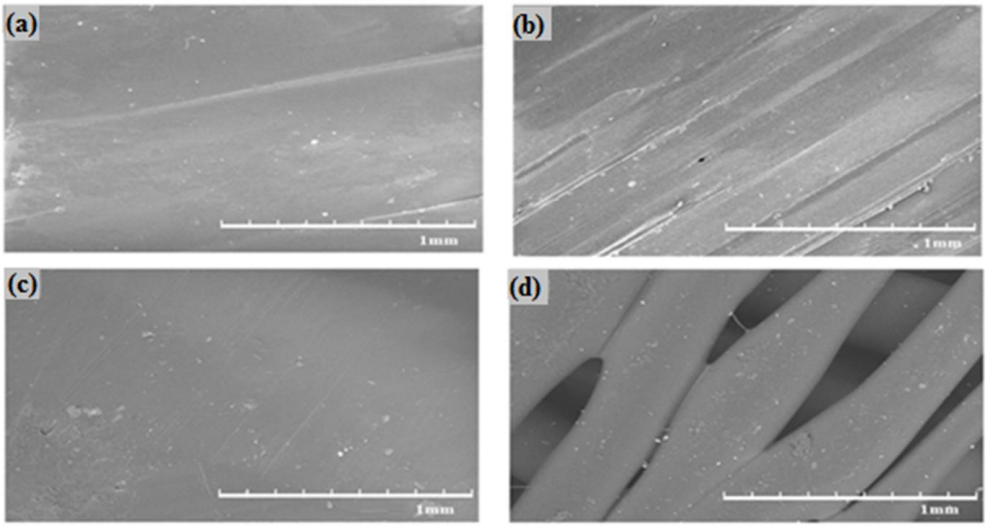

Figure 5.7: Scanning electron microscope (SEM) images of surface area of PLA/PCL composites. (a) PLA/PCL 100/0 wt.%, (b) PLA/PCL 75/25 wt.%, (c) PLA/PCL 25/75 wt.%, and (d) PLA/PCL 0/100 wt.%.

5.5 Effect of TiO_2 in PLA/PCL blend

Mechanical behavior of PLA/PCL/TiO_2 composites

To investigate the effect of TiO_2 in the mechanical properties of PLA/PCL composites, tensile strength testing was performed. The tensile strength decreased as the amount of TiO_2 increased, as can be observed in figure 5.8. As demonstrated in figure 5.5, the tensile stress of PLA/PCL blend (3:1 ratio) without TiO_2 has an approximate value of around 28 MPa. The addition of TiO_2 to the polymer blend enhances the mechanical properties; the highest tensile strength of the composite was created by mixing with 1 wt. % of TiO_2. However, a decrease in strength was observed when the amount of TiO_2 was increased to 3 and 5 wt.%. This is caused by the agglomeration of particles in the polymer matrix implying that the blend needs to be mixed with different methods or use a lower amount of TiO_2 to obtain better performance.

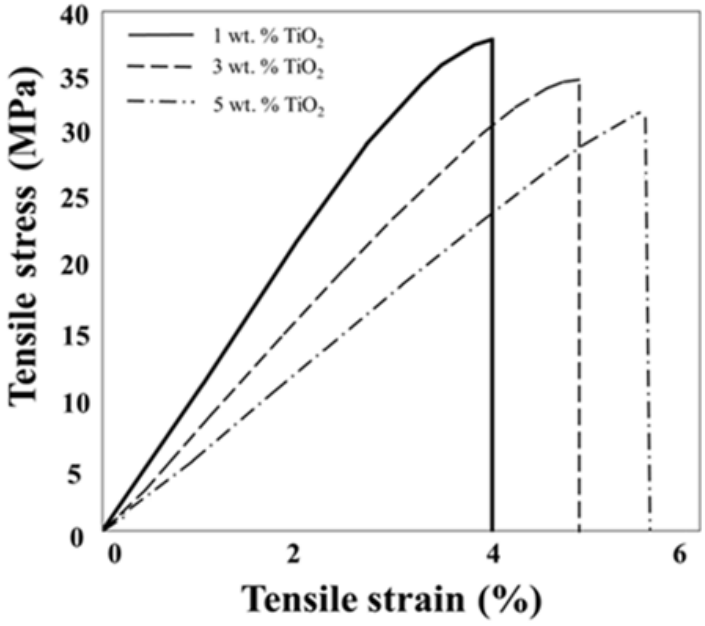

Figure 5.8: Stress-strain curve of PLA/PCL 75/25 wt.%, with different amounts of TiO_2 composites.

Fractography of PLA/PCL/TiO_2 composites

The fracture surface morphologies of PLA/PCL and PLA/PCL/TiO_2 composites were studied by scanning electron microscopy as shown in figures 5.9. It can be observed that TiO_2 particles are evenly dispersed in the PLA/PCL matrix even at a low concentration such as 1 wt. %. The photographic evidence observed in the SEM images correlates to the physical characteristics of the filaments. A brittle fracture surface showing little elongation of fibers and a porous, rough surface is seen in figure 5.9a. Contrarily in Figure 5.9b, a more fibrous fracture surface, indicating the elongation of the filament before breaking. Based on the evidence of images and measured properties, a higher tensile strength is expected in the PLA/PCL/TiO_2 composites.

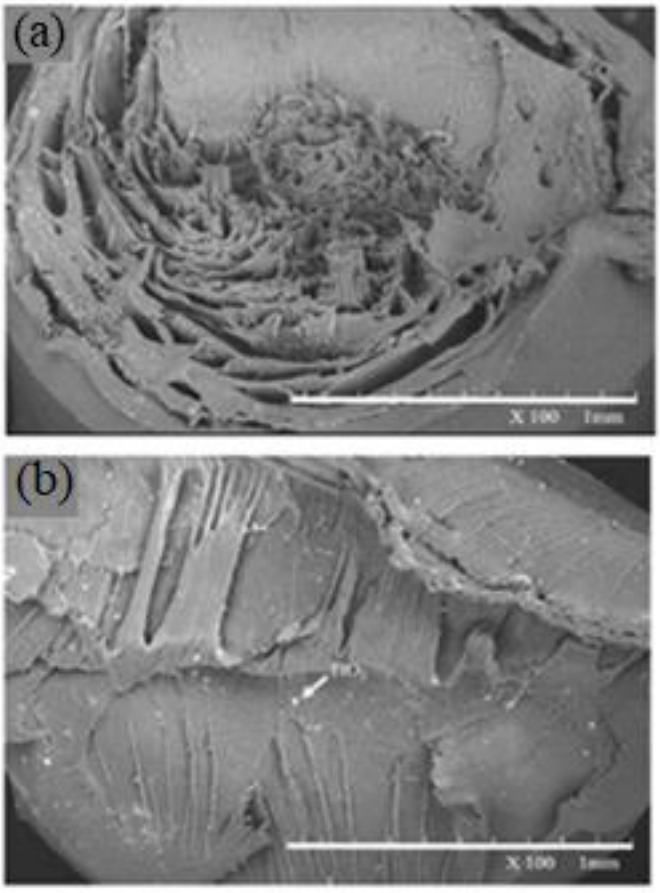

Figure 5.9: SEM images of (a) PLA/PCL 75/25 wt.%, (b) PLA/PCL/TiO2 74.25/24.75/1 wt.% (arrows indicate TiO_2).

5.6 Effect of particle size in PLA/PCL/TiO_2 composites

Mechanical behavior of PLA/PCL/TiO_2 composites

Tensile test results show the effect of TiO_2 in the blends in terms of mechanical properties and are graphically represented in figure 5.10 and figure 5.11. Ultimate tensile strength (UTS) increased when the three fillers were added to the polymer blend with the exception of the composites with 0.25 and 1 % of the large particles (figure 5.10). Similar results were found for the strain of the materials in terms of percent elongation (figure 5.11). There was an increase in the fracture strain when the TiO_2 was added, with the exception of 0.25 wt. % and 1 wt. % large particle. The increase in UTS and strain is expected due to the particles' interaction with the polymer matrix which in the case of the larger particle, having less surface area, is not as pronounced. Stress-strain curves of each composite were compared to the PLA/PCL baseline. These graphs are grouped in figure 5.12 and demonstrate little change in the modulus of elasticity with varying compositions. However, an increase in stress and fracture strain is observed due to the chains of the polymer elongating and arranging in the tensile test. As mentioned earlier, the effect of the larger particles on the stress-strain curves is less than those of the smaller particles.

Fractography of PLA/PCL/TiO_2 composites

Mechanical behavior of the printed specimens was analyzed by comparing their fracture surfaces using scanning electron microscopy. Samples chosen to examine were PLA/PCL 75/25 wt.% and composites with 0.5 % TiO_2 small, medium and large particles, since they are the ones with better mechanical properties. Micrographs in figure 5.13 show the fracture surface of these samples at different magnification and reveal the difference in ductility between them. PLA/PCL and PLA/PCL/TiO_2 large particle samples show small amount of plastic deformation consistent with stress-strain curves seen in figure 5.5 where they show the similar elastic modulus. Sample with small particles exhibits higher amount of plastic deformation, but less than the sample with medium particles. This is consistent with the mechanical testing values in figure 5.10 for UTS and figure 5.11 for fracture strain.

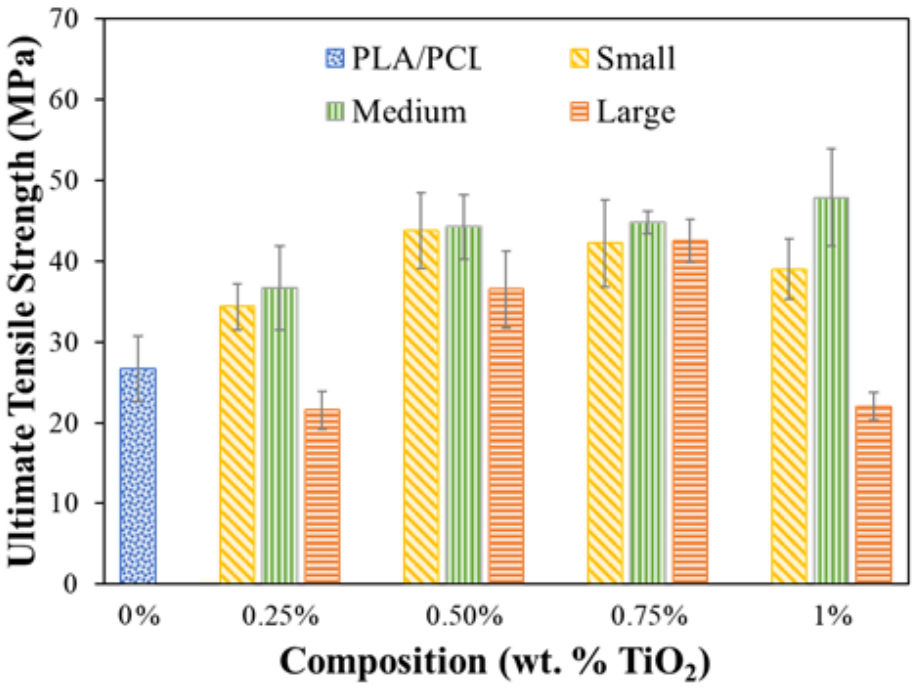

Figure 5.10: UTS values for PLA/PCL 75/25 wt.% blends with different TiO_2 compositions and particle sizes.

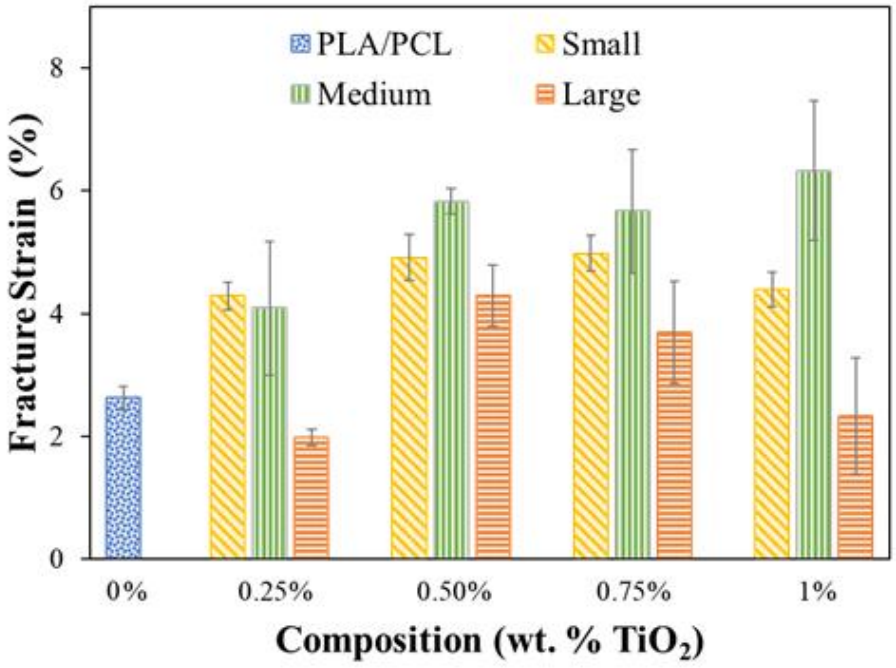

Figure 5.11: Percent elongation values for PLA/PCL 75/25 wt.% blends with different TiO_2 compositions and particle sizes.

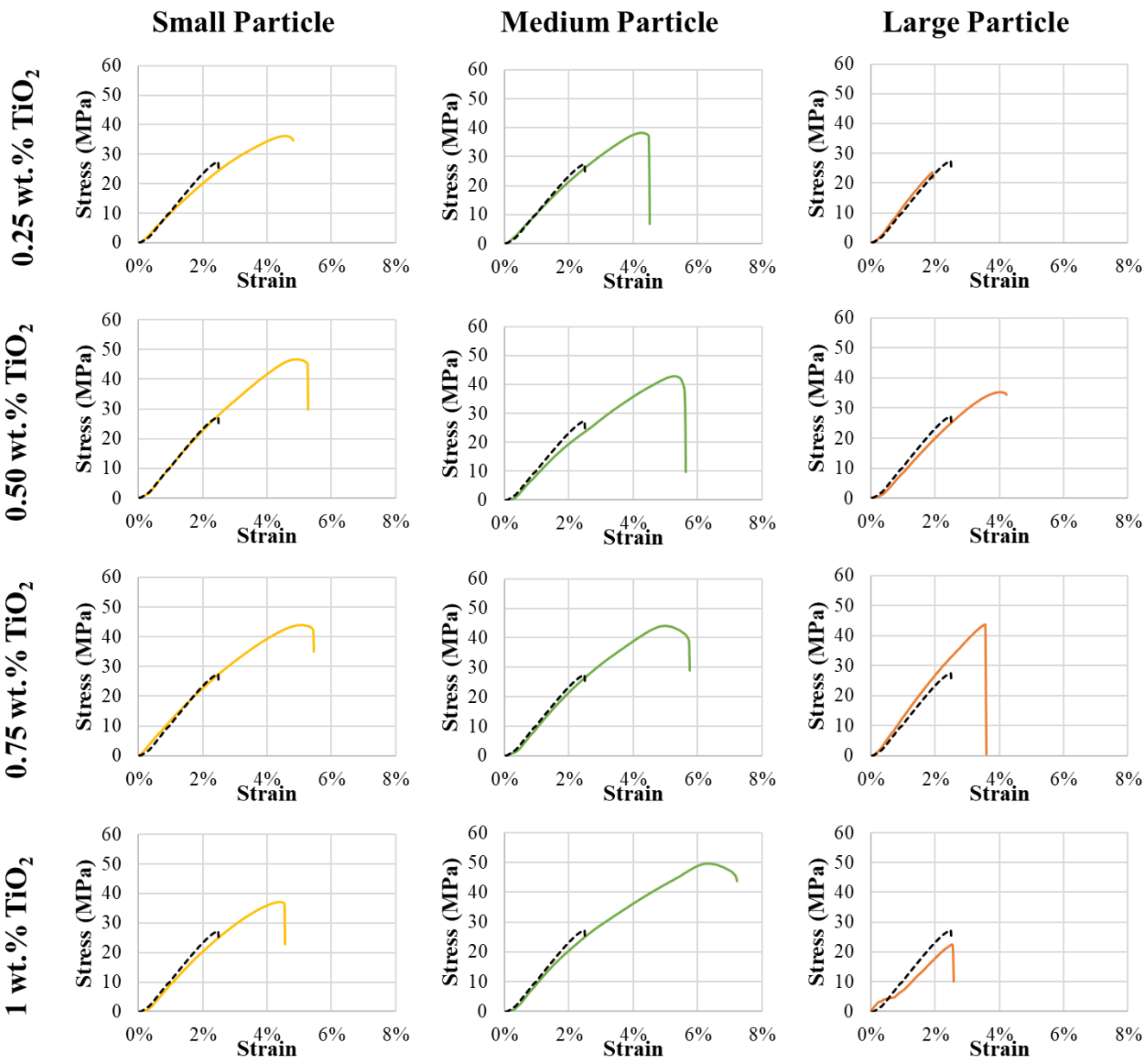

Figure 5.12: Stress-strain curves for the composites (solid lines) prepared for this study compared to the PLA/PCL 75/25 wt.% blend (black/dashed lines).

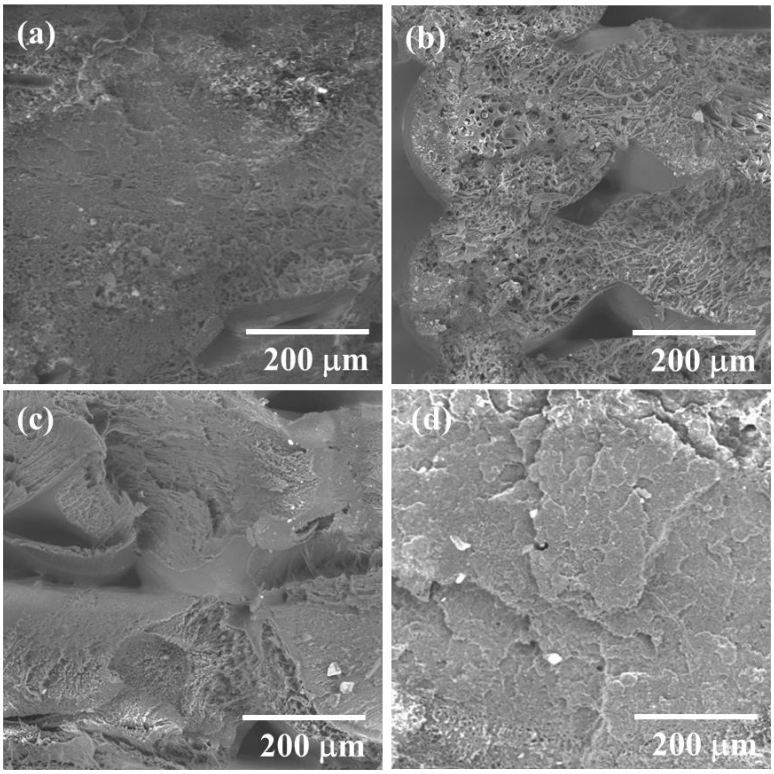

Figure 5.13: SEM micrographs of specimens composed of PLA/PCL and its composites. (a) PLA/PCL 75/25 wt.%, (b) PLA/PCL/TiO_2 74.6/24.9/0.5 wt.% TiO_2 small particles, (c) PLA/PCL/TiO_2 74.6/24.9/0.5 wt.% TiO_2 medium particles, (d) PLA/PCL/TiO_2 74.6/24.9/0.5 wt.% TiO_2 large particles.

5.7 In Vitro biocompatibility of PLA/PCL/TiO_2 composite

To evaluate the cellular effect of the PLA/PCL/TiO2 composites, MC3T3-E1 preosteoblast cells were cultured on samples without TiO2 and samples printed with 0.50 and 1 wt. % TiO2 medium particles since these were the ones with better mechanical properties. The cells were seeded onto the composites, and cell proliferation assay detected viable cells at 1, 2, 7 and 14 days post-seeding. Figure 5.14 indicates that the cell growth significantly increased in the PLA/PCL/TiO_2 composites in a time-dependent manner even though no appreciable difference was observed among the types of composites. Consistent with these results, the cells readily adhered and spread out on the surface of all types of PLA/PCL/TiO_2 composite (Figure 5.15). These data suggest that the PLA/PCL/TiO_2 composite can promote cell growth, and that the composites with different compositions used for the experiments do not present cytotoxicity.

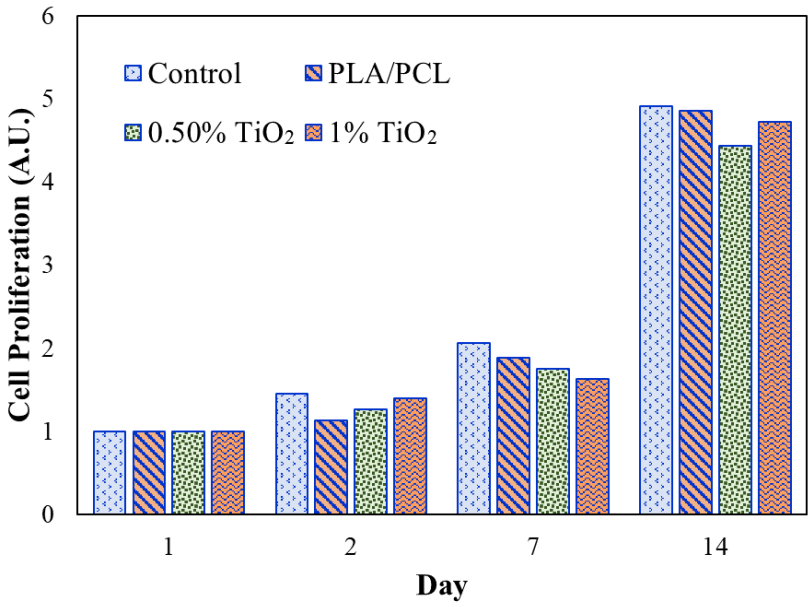

Figure 5.14: Effect of MC3T3-E1 cells proliferation on PLA/PCL 75/25 wt.%, PLA/PCL/TiO_2 74.6/24.9/0.5 wt.% TiO_2 medium particles and PLA/PCL/TiO_2 74.25/24.75/1 wt.% TiO_2 medium particles.

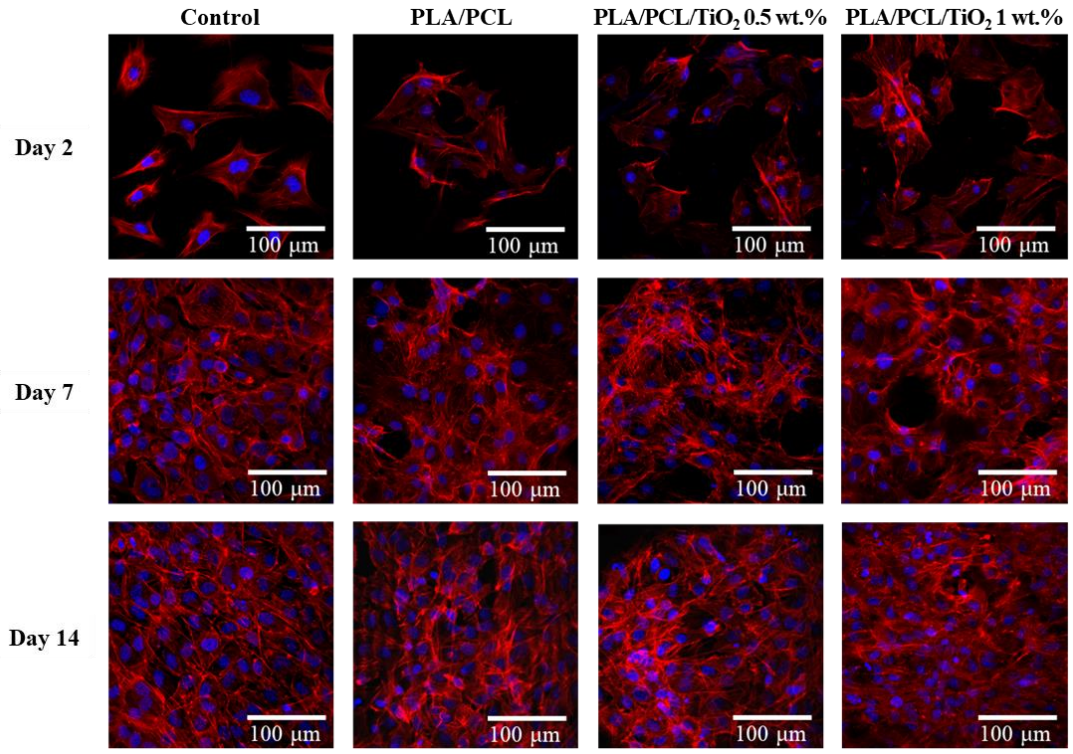

Figure 5.15: Effect of MC3T3-E1 cells adhesion and spreading of PLA/PCL 75/25 wt.%, PLA/PCL/TiO_2 74.6/24.9/0.5 wt.% TiO_2 medium particles and PLA/PCL/TiO_2 74.25/24.75/1 wt.% TiO_2 medium particles.

Given the robust cell proliferation and adhesion that was observed in PLA/PCL/TiO_2 composites, the effect of PLA/PCL/TiO_2 composites in osteoblast differentiation was investigated using MC3T3-E1 cells. As shown in figure 5.16, the ability of osteoblast differentiation was conducted with different types of PLA/PCL/TiO_2 composites and the disparity among the composites was not found. In addition, the relative mRNA expression of alkaline phosphatase (ALP) and osteocalcin (OCN), which are osteoblastic markers, was examined. The enhanced mRNA expression of ALP and OCN was observed in all the PLA/PCL/TiO_2 composites compared with that of the control (Figure 5.16c and d). It has been suggested that there are variable effects of TiO_2 in osteoblast differentiation depending on the size of particles blending with other materials; however, in our experiments the general tendency was an improved osteoblast differentiation by the addition of TiO_2 particles [43,44].

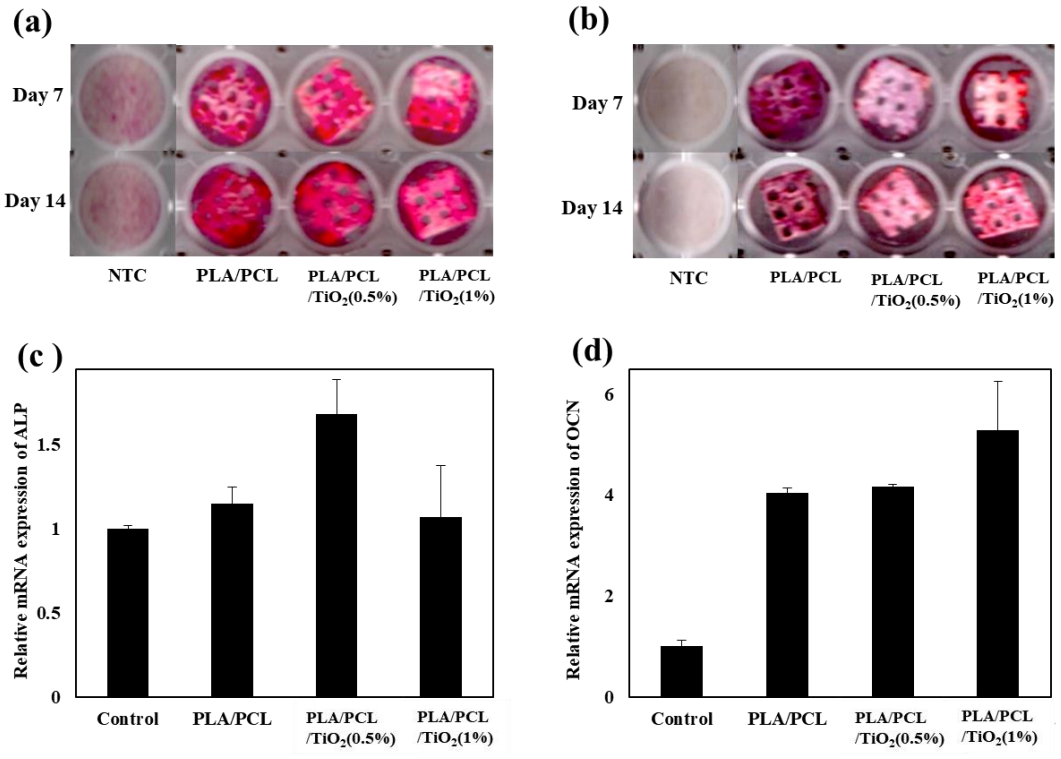

Figure 5.16: Osteoblast differentiation in PLA/PCL 75/25 wt.%, PLA/PCL/TiO_2 74.6/24.9/0.5 wt.% TiO_2 medium particles and PLA/PCL/TiO_2 74.25/24.75/1 wt.% TiO_2 medium particles. (a) Alkaline phosphatase staining (b) Alizarin red staining (c) Relative mRNA expression of osteoblast marker on differentiation day 7 of ALP and (d) OCN.

Taken together, the composites using PLA/PCL/TiO_2 have great biocompatibility including cell proliferation, adhesion and osteoblast differentiation that can improve the new strategy for printing 3D bone structure. To enforce the approach, we proposed the schematic design of 3D structure shown in figure 5.17. It displays the original bone structure which is divided into two parts due to the porosity of the bone (figure 5.17a). The outer part of the bone, called compact bone, has a dense structure with no obvious porosity. The inner part has many tiny spaces, and it is called spongy bone. Consistent with the structure of the original bone, it could be mimicked by two parts consisting of an outer part made with PLA/PCL/TiO_2 composites and the inner part which might be filled with soft fibers such as extracellular matrix (e.g. collagen) to build the open micro and nano-fluidic channel system.

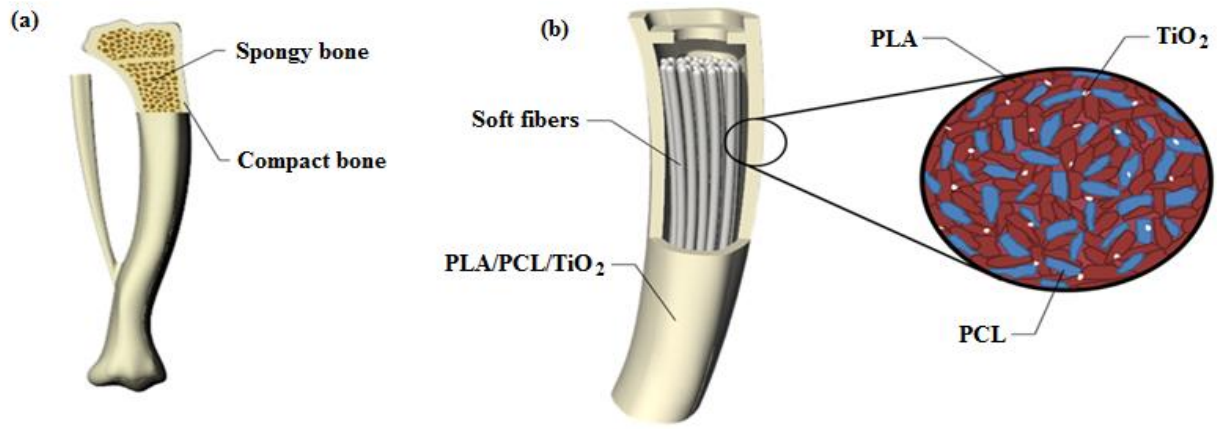

Figure 5.17: (a) Original bone structure, (b) Schematic design of artificial bone structure with PLA/PCL/TiO_2 and soft fibers.

Chapter 6: Conclusion

Biocompatible polymers have recently gained attention in the field of biomedical applications. Titanium base alloys have been commonly used for bone replacement procedures due to their biocompatible and the mechanical properties. However, the prosthetics which titanium base alloys present several disadvantages such as stress shielding and recurring pain to the subject [45]. The PLA/PCL composites infused with TiO_2 promise to be a better option for bone replacement and grafting procedures. In the present work, it has been demonstrated that Modified Fused Deposition Modeling is suitable for 3D printing multifunctional structures for artificial cancellous bone that have been difficult to manufacture with conventional methods.

Composites consisting of PLA, PCL and TiO_2 present good properties that can be used as bone substitute. Mechanical behavior of these composites was analyzed and the optimum composition (PLA/PCL/TiO2 0.50 % medium particles) was found. The strength of PLA/PCL 75/25 wt.% presents approximately 30 MPa and the modification of the blend with 0.5 wt.% of TiO_2 particles with an average size of 150 nm resulted in an increase of tensile strength up to 45 MPa due to the formation of an interface binding force among PLA, PCL and TiO_2. By adding this filler, the property of tensile stress has become similar to the cancellous bone (10-50 MPa) [46]. The effect of the total interface area has been studied indicating the optimum results with the maximum interface area making the melt blended composite for creating 3D printed bone structures. In addition to good mechanical properties, the composites do not exhibit cytotoxicity and can promote cell proliferation since there is no show of harmful effects on them. Overall, PLA/PCL/TiO_2 composites can mimic to such an extent the mechanical properties of the bone showing exceptional in vitro behavior.

In summary, the PLA/PCL/TiO_2 composite which mimics the cancellous bone was successfully printed using FDM and excellent in vitro biocompatibility of composites was demonstrated in this study. Furthermore, the biocompatibility and degradable properties might be enhanced through the addition of a soft filler such as component of extracellular matrix bearing

with hydroxyapatite and alginate [47,48]. Further research can be done to enhance these properties for future applications.

Works Cited

[1] F. Witte, Reprint of: The history of biodegradable magnesium implants: A review, Acta Biomater. 23 (2015) S28–S40. doi:10.1016/j.actbio.2015.07.017.

[2] a S. Brydone, D. Meek, S. Maclaine, Bone grafting, orthopaedic biomaterials, and the clinical need for bone engineering., Proc. Inst. Mech. Eng. H. 224 (2010) 1329–1343. doi:10.1243/09544119JEIM770.

[3] K. Choi, J.L. Kuhn, M.J. Ciarelli, S.A. Goldstein, The elastic moduli of human subchondral, trabecular, and cortical bone tissue and the size-dependency of cortical bone modulus, J. Biomech. 23 (1990) 1103–1113. doi:10.1016/0021-9290(90)90003-L.

[4] Y.N. Yeni, C.U. Brown, Z. Wang, T.L. Norman, The influence of bone morphology on fracture toughness of the human femur and tibia, Bone. 21 (1997) 453–459. doi:10.1016/S8756-3282(97)00173-7.

[5] S.J. Hollister, Porous scaffold design for tissue engineering., Nat. Mater. 4 (2005) 518–24. doi:10.1038/nmat1421.

[6] J.J. Klawitter, S.F. Hulbert, Application of porous ceramics for the attachment of load bearing internal orthopedic applications, J. Biomed. Mater. Res. 5 (1971) 161–229. doi:10.1002/jbm.820050613.

[7] V. Sansone, D. Pagani, M. Melato, The effects on bone cells of metal ions released from orthopaedic implants. A review., Clin. Cases Miner. Bone Metab. 10 (2013) 34–40. doi:10.11138/ccmbm/2013.10.1.034.

[8] H.S. Brar, M.O. Platt, M. Sarntinoranont, P.I. Martin, M. V. Manuel, Magnesium as a biodegradable and bioabsorbable material for medical implants, Jom. 61 (2009) 31–34. doi:10.1007/s11837-009-0129-0.

[9] L. Tan, X. Yu, P. Wan, K. Yang, Biodegradable Materials for Bone Repairs: A Review, J. Mater. Sci. Technol. 29 (2013) 503–513. doi:10.1016/j.jmst.2013.03.002.

[10] D.F. Williams, On the nature of biomaterials, Biomaterials. 30 (2009) 5897–5909. doi:10.1016/j.biomaterials.2009.07.027.

[11] E.S. Place, J.H. George, C.K. Williams, M.M. Stevens, Synthetic polymer scaffolds for tissue engineering, Chem Soc Rev. 38 (2009) 1139–1151. doi:10.1039/b811392k.

[12] Y. Cheng, S. Deng, P. Chen, R. Ruan, Polylactic acid (PLA) synthesis and modifications: a review, Front. Chem. China. 4 (2009) 259–264.

[13] B.J.R.F. Bolland, J.M. Kanczler, P.J. Ginty, S.M. Howdle, K.M. Shakesheff, D.G. Dunlop, R.O.C. Oreffo, The application of human bone marrow stromal cells and poly(dl-lactic acid) as a biological bone graft extender in impaction bone grafting, Biomaterials. 29 (2008) 3221–3227. doi:10.1016/j.biomaterials.2008.04.017.

[14] X. Wen, P.A. Tresco, Fabrication and characterization of permeable degradable poly(dl-lactide-co-glycolide) (PLGA) hollow fiber phase inversion membranes for use as nerve tract guidance channels, Biomaterials. 27 (2006) 3800–3809. doi:10.1016/j.biomaterials.2006.02.036.

[15] K. Halász, L. Csóka, Plasticized biodegradable poly (lactic acid) based composites containing cellulose in micro-and nanosize, J. Eng. 2013 (2012).

[16] M. Santosh, V.S. Karuppudaiyan, M.T.S.A.S. G, S. Eshraghi, S. Das, P.K. Ilankeeran, P.M. Mohite, S. Kamle, T.P. Quinn, T.L. Oreskovic, C.N. McCowan, N.R. Washburn, Mechanical & Microstructural Properties of PCL Scaffolds with 1-D, 2-D & 3-D Orthogonally Oriented Porous Architectures Produced by Selective Laser Sintering, Acta Biomater. 6 (2011) 2467–2476. doi:10.1016/j.actbio.2010.02.002.Mechanical.

[17] E. Govor, V. Oceli, M. Slouf, A. Šitum, Characterization of Biodegradable Polycaprolactone Containing Titanium Dioxide Micro and, 8 (2014) 577–581.

[18] J. Zhang, W. Song, J. Guo, J. Zhang, Z. Sun, L. Li, F. Ding, M. Gao, Cytotoxicity of different sized TiO 2 nanoparticles in mouse macrophages, (n.d.). doi:10.1177/0748233712442708.

[19] M. Hamzeh, G.I. Sunahara, In vitro cytotoxicity and genotoxicity studies of titanium dioxide (TiO 2) nanoparticles in Chinese hamster lung fibroblast cells, (2013). doi:10.1016/j.tiv.2012.12.018.

[20] Q. Yu, H. Wang, Q. Peng, Y. Li, Z. Liu, M. Li, Different toxicity of anatase and rutile TiO2 nanoparticles on macrophages: Involvement of difference in affinity to proteins and phospholipids, J. Hazard. Mater. 335 (2017) 125–134. doi:10.1016/J.JHAZMAT.2017.04.026.

[21] Z. Wei, L. Chen, D.M. Thompson, L.D. Montoya, Effect of particle size on in vitro cytotoxicity of titania and alumina nanoparticles, (n.d.). doi:10.1080/17458080.201.

[22] L. Visai, L. de Nardo, C. Punta, L. Melone, A. Cigada, M. Imbriani, C.R. Arciola, Titanium oxide antibacterial surfaces in biomedical devices, Int. J. Artif. Organs. 34 (2011) 929–946. doi:10.5301/ijao.5000050.

[23] J.P. Mofokeng, A.S. Luyt, Morphology and thermal degradation studies of melt-mixed poly(hydroxybutyrate-co-valerate) (PHBV)/poly(??-caprolactone) (PCL) biodegradable polymer blend nanocomposites with TiO2 as filler, J. Mater. Sci. 50 (2015) 3812–3824. doi:10.1007/s10853-015-8950-z.

[24] A.K. Amert, D.-H. Oh, N.-S. Kim, A simulation and experimental study on packing of nanoinks to attain better conductivity, J. Appl. Phys. 108 (2010) 102806. doi:10.1063/1.3511687.

[25] J. Hoffman, S. Hwang, A. Ortega, N.-S. Kim, K. Moon, The Standardization of Printable Materials and Direct Writing Systems, J. Electron. Packag. 135 (2013) 11006.

doi:10.1115/1.4023809.

[26] N.-S. Kim, K.N. Han, Future direction of direct writing, J. Appl. Phys. 108 (2010) 102801. doi:10.1063/1.3510359.

[27] K.H.C. N. S. Kim, K. N. Han, Direct Writing Technology for 21st Century Industries - Focus on Micro-Dispensing Deposition Write Technology, Trans. KSMTE Spring Conf. (2007) 511–515.

[28] N.P. Kim, J.-S. Eo, D. Cho, Optimization of piston type extrusion (PTE) techniques for 3D printed food, J. Food Eng. 235 (2018) 41–49. doi:10.1016/J.JFOODENG.2018.04.019.

[29] S. Hong, N. Kim, Synthesis of 3D Printable Cu–Ag Core–Shell Materials: Kinetics of CuO Film Removal, J. Electron. Mater. 44 (2015) 823–830. doi:10.1007/s11664-014-3588-1.

[30] K.N. Han, N.S. Kim, Challenges and Opportunities in Direct Write Technology Using Nano-metal Particles, KONA Powder Part. J. 27 (2009) 73–83. doi:10.14356/kona.2009009.

[31] L.H. Sperling, Polymer Surfaces and Interfaces: The Need for Uniform Terminology, ACS Div. Polym. Mater. Sci. Eng. (1995). http://www.polyacs.org/612.html (accessed September 26, 2016).

[32] E. Helfand, Y. Tagami, Theory of the Interface Between Immiscible Polymers, J. Chem. Phys. II J. Chem. Phys. Phys. E. F. Riebling, J. Chern. Phys. 57 (1972). doi:10.1063/1.1677735.

[33] DSC 404 F1 Pegasus® - NETZSCH Analyzing & Testing, (n.d.). https://www.netzsch-thermal-analysis.com/us/products-solutions/simultaneous-thermogravimetry-differential-scanning-calorimetry/dsc-404-f1-pegasus/ (accessed April 22, 2018).

[34] Hitachi High-Technologies Announces Shipments of Tabletop Microscope TM-1000 Surpass 1,000 Units | Business Wire, (n.d.). https://www.businesswire.com/news/home/20090930005411/en/Hitachi-High-Technologies-Announces-Shipments-Tabletop-Microscope-TM-1000 (accessed April 21, 2018).

[35] 100 Series Electromechanical Universal Test Machine, (n.d.). https://www.testresources.net/test-machines/universal-testing-machines/100-series-universal-test-machine/ (accessed April 19, 2018).

[36] Low Cost Solution for PAMPA Assays - Using the Epoch™ Microplate Spectrophotometer with pION's PAMPA Explorer™ for the In-vitro Drug Permeability Studies, (n.d.). https://www.biotek.pt/pt/resources/application-notes/low-cost-solution-for-pampa-assays-using-the-epoch-microplate-spectrophotometer-with-pions-pampa-explorer-for-the-in-vitro-drug-permeability-studies/ (accessed April 22, 2018).

[37] ZEISS LSM 700 for Life Sciences from ZEISS Microscopy | SelectScience, (n.d.). http://www.selectscience.net/products/zeiss-lsm-700-for-life-sciences/?prodID=92819 (accessed April 22, 2018).

[38] StepOne & StepOnePlus Real-Time PCR Systems, (n.d.). https://www.thermofisher.com/us/en/home/life-science/pcr/real-time-pcr/real-time-pcr-instruments/step-one-real-time-pcr-systems.html (accessed April 22, 2018).

[39] S. Saeidlou, M.A. Huneault, H. Li, C.B. Park, Poly(lactic acid) crystallization, Prog. Polym. Sci. 37 (2012) 1657–1677. doi:10.1016/j.progpolymsci.2012.07.005.

[40] A.M. Harris, E.C. Lee, Improving mechanical performance of injection molded PLA by controlling crystallinity, J. Appl. Polym. Sci. 107 (2008) 2246–2255. doi:10.1002/app.27261.

[41] V. Khoshkava, M.R. Kamal, Effect of Surface Energy on Dispersion and Mechanical Properties of Polymer/Nanocrystalline Cellulose Nanocomposites, Biomacromolecules. 14 (2013) 3155–3163. doi:10.1021/bm400784j.

[42] B. a Ibrahim, K.M. Kadum, Influence of Polymer Blending on Mechanical and Thermal Properties, Mod. Appl. Sci. 4 (2010) 157–161. doi:10.5539/mas.v4n9p157.

[43] P. Santiago-Medina, P.A. Sundaram, N. Diffoot-Carlo, Titanium Oxide: A Bioactive Factor in Osteoblast Differentiation, Int. J. Dent. 2015 (2015) 1–9. doi:10.1155/2015/357653.

[44] H. Pullisaar, H. Tiainen, M.A. Landin, S.P. Lyngstadaas, H.J. Haugen, J.E. Reseland, E. Ostrup, Enhanced in vitro osteoblast differentiation on TiO2 scaffold coated with alginate hydrogel containing simvastatin., J. Tissue Eng. 4 (2013) 2041731413515670. doi:10.1177/2041731413515670.

[45] A. Besinis, T. De Peralta, R.D. Handy, The antibacterial effects of Ag, TiO2 and SiO2 nanoparticles compared to the Dental Disinfectant Chlorhexidine on Streptococcus mutans Using a Suite of Bioassays., Nanotoxicology. 8 (2012) 1–45. doi:10.3109/17435390.2012.742935.

[46] O. Hospital, A. N, Tensile and Compressive Properties of Cancellous Bone, J. Biomech. 24 (1991) 1143–1149.

[47] A. Bayrak, M. Tyralla, J. Ladhoff, M. Schleicher, U.A. Stock, H.D. Volk, M. Seifert, Human immune responses to porcine xenogeneic matrices and their extracellular matrix constituents in vitro, Biomaterials. 31 (2010) 3793–3803. doi:10.1016/j.biomaterials.2010.01.120.

[48] S.F. Badylak, The extracellular matrix as a biologic scaffold material, Biomaterials. 28 (2007) 3587–3593. doi:10.1016/j.biomaterials.2007.04.043.

Vita

Sandra Elena Nájera Beltrán was born on June 25, 1993 in Ciudad Juárez, México. She graduated from El Chamizal High School in Ciudad Juárez in the Spring of 2011. In Fall 2011 she enrolled at El Paso Community College and then transferred to the University of Texas at El Paso, where she graduated with a Bachelor of Science in Metallurgical and Materials Engineering in Spring 2016. During her studies as a bachelor, she got the opportunity to work as a Research Assistant in Printing Nano Engineering lab (PNE) under the direction of Dr. Nam-Soo Kim. Dr. Kim encouraged her to continue her studies as a master's student. In the Summer of 2016, she entered the graduate school at the University of Texas at El Paso in the Department of Metallurgical, Materials and Biomedical Engineering. After enrolling, Dr. Kim offered her to participate in a Study Abroad program. In Fall 2016 she was a student at the University of Ulsan in South Korea, where she was also conducting research at their campus. In Spring 2017 she returned to UTEP and continued her studies and research project. She published two papers as a first author and won the "Graduate Research Award" from the Department of Metallurgical, Materials and Biomedical Engineering in Spring 2018.

Permanent address: Obreros, Cd. Juárez, Chihuahua
México, 32425

This thesis was typed by Sandra Nájera.